

Nanoparticles

A Facile Molecular Precursor-based Synthesis of Ag₂Se Nanoparticles and Its Composites with TiO₂ for Enhanced Photocatalytic Activity

Shashank Mishra,^{*[a]} Dan Du,^[a, b] Erwann Jeanneau,^[c] Frederic Dappozze,^[a] Chantal Guillard,^[a] Jinlong Zhang,^[b] and Stéphane Daniele^[a]

Abstract: The reactions of different silver(I) reagents AgX (X⁻=iodide, trifluoroacetate, triflate) with selenoethers R₂Se (R=Me, tBu) in a variety of solvents were investigated in relation with their use as precursors for Ag₂Se nanomaterials. Different reaction conditions led to different reactivities and afforded either molecular complexes or metal selenide nanoparticles. The reactions leading to in situ formation of the metal selenide nanoparticles were then extended in the presence of commercial TiO₂ (P25) to prepare silver selenide–titania nanocomposites with different Ag/Ti ratios. These nanocomposites, well characterized by elemental analysis (Ag, Se), PXRD, TEM, BET, XPS and UV/Vis studies, were investigated as photocatalysts for the degradation of formic acid (FA) solution. The xAg₂Se-TiO₂ nanocomposites ($x=0.01$, 0.13 and 0.25 mol%) exhibited a much higher catalytic activity as compared to P25, which is an established benchmark for the photocatalysis under UV light, and retained a good photocatalytic stability after recycling for several times.

Silver chalcogenides with their narrow band gaps (0.9, 0.15 and 0.67 eV for Ag₂S, Ag₂Se and Ag₂Te, respectively) form an extremely important class of semiconductors with applications not only in microelectronics but also in thermoelectric, solid electrolytes in secondary batteries and as quantum dots in biomedical imaging.^[1–3] Among these, silver selenide shows many

interesting and useful properties.^[4] There are two stable crystalline phases at atmospheric pressure: the high-temperature α -Ag₂Se with a body-centered cubic structure and low-temperature β -Ag₂Se with an orthorhombic structure.^[5] The α -Ag₂Se is a well-known superionic conductor that is useful as the solid electrolyte in photo-chargeable secondary batteries.^[4] The β -Ag₂Se, on the other hand, is a narrow band-gap semiconductor which has been widely used as a photosensitizer in photographic films or thermochromic materials.^[6] Selection of a suitable synthetic route to these nanomaterials is crucial as their properties may evolve during the preparation. Several methods have been employed to obtain different forms of Ag₂Se nanomaterials. Liu et al. synthesized monodispersed Ag₂Se nanoparticles (NPs) of 60–80 nm in length and 30–40 nm in width by a hydrothermal reaction using AgNO₃ and Na₂SeSO₃ in the presence of poly(vinyl pyrrolidone) (PVP) and KI at 180 °C for 20 h.^[7] On the other hand, Li et al. used bulk selenium (Se) powder and silver (Ag) foil in a solvothermal process (10 h at 160 °C in methanol or ethanol in an autoclave) to obtain films of Ag₂Se dendrites of highly oriented (001) nanocrystals.^[8] Zhu et al. used a hot injection method employing TOPSe (Se dissolved in tri-octylphosphine) to prepare Ag₂Se quantum dots (QDs).^[9] Yao et al. prepared an Ag₂Se aerogel by an ion-exchange reaction of a monolithic CdSe wet gel, followed by its supercritical drying.^[10] Soft chemical routes such as chemical vapor deposition (CVD), metal–organic decomposition (MOD), and the sol–gel process are preferred for the elaboration of nanomaterials due to the number of advantages they offer.^[11] These procedures need well-characterized single-source precursors (SSPs) with certain properties.^[12] However, well-characterized metal–organic single-source precursors for Ag₂Se nanomaterials are scarce.^[13] Very often, these reported SSPs require high temperature to be converted into Ag₂Se nanomaterials. Recently, selenoethers have been shown as a simple but effective source for obtaining selenium-containing chalcopyrite semiconducting materials. Several reports have appeared recently employing either metal complexes with these selenoethers as single-source precursors,^[14] or reactions of these selenoethers R₂Se (R=Me, Et, tBu) with metal halides/oxohalides/alkyls using the CVD technique,^[15–17] to obtain high-quality metal solenoid films. However, so far the selenoethers have been used only to obtain thin films, requiring high temperature. There is no report available on the use

[a] Dr. S. Mishra, D. Du, F. Dappozze, Dr. C. Guillard, Prof. S. Daniele

Université Lyon 1

IRCELYON, CNRS-UMR 5256

2 Avenue A. Einstein, 69626 Villeurbanne (France)

Fax: (+33) 472445399

E-mail: shashank.mishra@ircelyon.univ-lyon1.fr

[b] D. Du, Prof. J. Zhang

Key Laboratory for Advanced Materials and Institute of Fine Chemicals

East China University of Science and Technology

130 Meilong Road, Shanghai 200237 (China)

[c] Dr. E. Jeanneau

Université Lyon 1

Centre de Diffraction Henri Longchambon

5 rue de La Doua, 69100 Villeurbanne (France)

Supporting information and the ORCID identification number(s) for the author(s) of this article can be found under <http://dx.doi.org/10.1002/asia.201600157>.

of these selenoethers to obtain NPs, particularly at room temperature.

Due to its low cost, non-toxicity, chemical stability, and high activity, TiO_2 has been widely investigated as one of the most promising photocatalysts. However, an easy recombination of the photogenerated electron/hole (e^-/h^+) reduces its catalytic efficiency.^[18] To enhance the photocatalytic performance, efforts have been made to modify the titania by doping it with metals or non-metallic elements.^[19] A considerable enhancement in the photocatalytic efficiency of TiO_2 under visible light has been reported by coupling TiO_2 with another low bandgap semiconductor such as CdS ,^[20] CdSe ,^[21] AgX ^[22] and Ag_2S .^[23] To the best of our knowledge, there is no report on the photocatalysis of $\text{Ag}_2\text{Se}-\text{TiO}_2$ composites, although Meng et al. recently reported the preparation of an Ag_2Se -graphene/ TiO_2 composite which showed a red-shifted absorption and better visible-light photocatalytic activity for the degradation of rhodamine B (RhB) than pure TiO_2 .^[24] In this paper, we describe interesting and divergent reactivities of selenoethers R_2Se ($\text{R}=\text{Me}$, $t\text{Bu}$) with different silver reagents which not only lead to the formation and isolation of new molecular complexes as SSPs for silver selenide nanomaterials but, more importantly, also result in the direct synthesis of $\beta\text{-Ag}_2\text{Se}$ NPs at room temperature. This facile method of the synthesis of narrow band-gap semiconducting $\beta\text{-Ag}_2\text{Se}$ NPs was then used to obtain nanocomposites with TiO_2 which showed much improved photocatalytic activity compared to that of pure TiO_2 (P25) for the degradation of formic acid (FA) under UV irradiation. The commercially available P25 is an established benchmark for photocatalysis under UV light, and there are very few reports available presenting improvements on its photocatalytic activity.

Reactions of selenoethers R_2Se ($\text{R}=\text{Me}$, $t\text{Bu}$) with different silver(I) reagents were explored in different solvents in relation with their use as possible precursors for Ag_2Se nanomaterials. Addition of $t\text{Bu}_2\text{Se}$ to AgTFA (where $\text{TFA}=\text{trifluoroacetate}$) at room temperature in diethylether resulted in a gradual change in the color of the solution, from colorless to light brown and then to dark brown. Finally, black Ag_2Se NPs were precipitated after 30 min of the reaction. An intermediate molecular species, $[\text{Ag}(\text{TFA})(t\text{Bu}_2\text{Se})_2]$ (**1**), could be trapped within few minutes of the reaction and characterized spectroscopically and by X-ray crystallography. The same species was isolated if the reaction was carried out in anhydrous ethanol or tetrahydrofuran (THF). However, on prolonged stirring of 30–60 min, the THF solution first turned brown and finally black to give Ag_2Se NPs. With silver triflate (AgOTf), the selenoether $t\text{Bu}_2\text{Se}$ afforded Ag_2Se NPs immediately at room temperature, irrespective of the nature of the solvent used (hexane, diethylether, THF). By contrast, the reactions of $t\text{Bu}_2\text{Se}$ with silver iodide (in dichloromethane) or that of Me_2Se with silver trifluoroacetate (in THF) were straightforward and led to the isolation of the molecular complexes $[\text{Ag}_4\text{I}_4(t\text{Bu}_2\text{Se})_4]$ (**2**) and $[\text{Ag}_5(\text{TFA})_5(\text{Me}_2\text{Se})_4]$ (**3**), respectively. Unlike the derivative **1** which turns gradually black even when kept in the dark and under inert atmosphere, apparently due to the formation of Ag_2Se NPs, the precursors **2** and **3** are stable at room temperature. While precursors **1** and **3** are highly soluble in common organic solvents, the

silver iodide derivative **2** shows limited (dichloromethane) to poor solubility (THF, toluene, hexane). It should be noted that the coordination chemistry of silver with neutral selenide-containing ligands remains least explored.^[25]

The isolated colorless precursors **1**–**3** were characterized by the elemental analysis, FT-IR, and NMR (^1H , ^{13}C , ^{77}Se) spectroscopy as well as single-crystal X-ray diffraction. The FT-IR spectra of **1** and **3** (Figure S1 in the Supporting Information) exhibit characteristic bands for the trifluoroacetate and $t\text{Bu}_2\text{Se}/\text{Me}_2\text{Se}$ ligands. The trifluoroacetate ligand may bind to the metal center in a number of fashions, and the asymmetric and symmetric vibrations of the CO_2 group can indicate its binding modes.^[26] The appearance of only a single band at 1670 cm^{-1} for ν_{as} CO_2 is consistent with one type of TFA ligand present in **1**, whereas an overlap of the same absorption due to three different bonding modes of the TFA ligand results in a strong broad band centered around 1680 cm^{-1} in **3** (Figure 1). The derivative **2** shows characteristic peak(s) for the $t\text{Bu}_2\text{Se}$ ligand only, as metal-iodide stretching usually appears below 400 cm^{-1} . As expected, the ^1H NMR spectra of **1**–**3** in $\text{CDCl}_3/\text{CD}_2\text{Cl}_2$ are simple and show only a singlet at $\delta=1.57\text{--}1.95\text{ ppm}$ for the $t\text{Bu}/\text{Me}$ groups of the selenoethers.

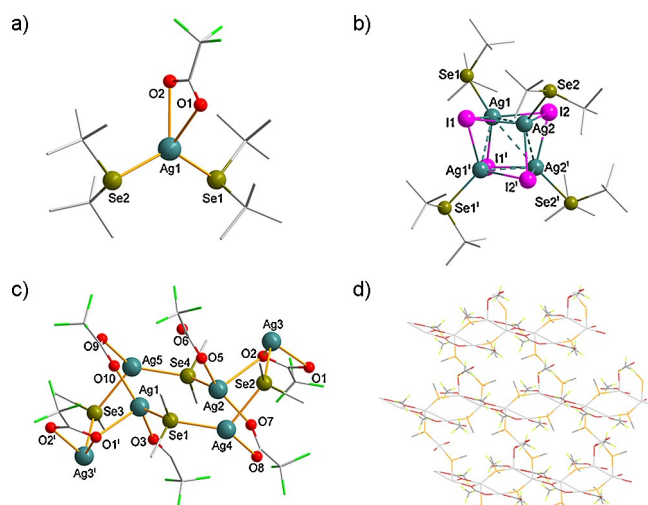


Figure 1. (a)–(c) Perspective view of the molecular structures of **(1)**–**(3)** with 30% probability ellipsoids. H atoms on alkyl group are omitted for clarity. (d) Extended structure of **(3)**. Selected bond lengths [\AA] and angles [$^\circ$]: (1): $\text{Ag1}-\text{O1}$ 2.524(9), $\text{Ag1}-\text{O2}$ 2.495(9), $\text{Ag1}-\text{Se1}$ 2.588(1), $\text{O1}-\text{Ag1}-\text{O2}$ 52.0(3), $\text{Se1}-\text{Ag1}-\text{Se2}$ 124.41(5), $\text{O1}-\text{Ag1}-\text{Se1}$ 110.4(3). (2): $\text{I1}-\text{Ag1i}$ 2.8693(4), $\text{I1}-\text{Ag2}$ 2.9367(4), $\text{Ag1}-\text{Ag2i}$ 3.3609(5), $\text{Ag1}-\text{Ag1i}$ 3.1566(6), $\text{Ag1}-\text{I2i}$ 2.8705(4), $\text{Ag1} \cdots \text{Ag2}$ 3.0719(5), $\text{Ag1}-\text{Se1}$ 2.6362(5), $\text{Ag2} \cdots \text{Ag2i}$ 3.2328(7), $\text{Ag2}-\text{I2}$ 2.8714(4), $\text{I1}-\text{Ag1}-\text{Se1}$ 98.01(1), $\text{I1i}-\text{Ag1}-\text{Se1}$ 118.38(1), $\text{I1}-\text{Ag2}-\text{I2i}$ 114.39(1), $\text{I1}-\text{Ag1}-\text{I1i}$ 109.98(1). (3): $\text{O1}-\text{Ag1}$ 2.574(16), $\text{O7}-\text{Ag2}$ 2.218(14), $\text{O9}-\text{Ag4}$ 2.444(12), $\text{Se1}-\text{Ag1}$ 2.696(3), $\text{Se2}-\text{Ag3}$ 2.541(3), $\text{Ag1} \cdots \text{Ag5}$ 3.138(2), $\text{Ag2} \cdots \text{Ag4}$ 3.188(2), $\text{O1}-\text{Ag1}-\text{O3}$ 98.8(5), $\text{O5}-\text{Ag2}-\text{O7}$ 145.5(6), $\text{O9}-\text{Ag4}-\text{O8}$ 75.4(4), $\text{Se4}-\text{Ag2}-\text{Se2}$ 161.71(9), $\text{Se2}-\text{Ag4}-\text{Se1}$ 119.63(9), $\text{O1}-\text{Ag1}-\text{Se1}$ 86.6(3). Symmetry elements, (2): (i) $-x+1, y, -z+1/2$, (3): (i) $x-1/2, -y+1/2, z-1/2$.

The monomeric $[\text{Ag}(\text{TFA})(t\text{Bu}_2\text{Se})_2]$ (**1**) and tetrameric $[\text{Ag}_4\text{I}_4(t\text{Bu}_2\text{Se})_4]$ (**2**), which crystallize in the triclinic space group $\bar{P}\bar{1}$ (with $R_1=0.074$ and $wR_2=0.156$) and the monoclinic space group $C2/c$ (with $R_1=0.025$ and $wR_2=0.045$), respectively, have the $t\text{Bu}_2\text{Se}$ ligand bonded in a terminal fashion (Figure 1). In **1**,

the TFA group is bonded in a chelating manner to afford a 4-coordinate silver center. Except for a small bond angle, O1-Ag1-O2 52.0(3) $^{\circ}$ (due to small bite angle of the TFA ligand), other Se-Ag1-Se and Se-Ag1-O angles are in the range 110.4(3)–124.41(5) $^{\circ}$, thus indicating a distorted tetrahedral environment around the silver center. The tetrameric structure of **2** has the Ag and I atoms alternating in a distorted cubane-like AgI core where the tBu₂Se ligands cap the Ag corners. Each face is distorted due to argentophilic Ag···Ag interactions (3.072–3.361 Å) that makes the average Ag···Ag atomic separation shorter than the average I···I atomic separation by more than 1 Å. The Ag–Se bond length, 2.588(1)–2.646(5) Å, is consistent with the literature value on terminal-bonded selenium-containing ligands.^[27] The 2D sheet structure of **3**, which crystallizes in the monoclinic space group *P*₂/*n* (with *R*=0.116 and *wR*=0.178), is composed of the [Ag₅(μ₃-η¹,η¹,η¹-TFA)₂(μ-η²,η¹-TFA)(η¹-TFA)₂(μ-Me₂Se)₄] building block. This structure can be seen formally as the association between [Ag₄(μ-Me₂Se)₂(μ₃-η¹:η¹:η¹-TFA)₂(η¹-TFA)] and [Ag(μ-Me₂Se)₂(μ-η²:η¹-TFA)₂] units via μ-Me₂Se and one oxygen atom of μ,η²:η¹-TFA ligands (Figure S2a in the Supporting Information). The silver atoms and bridging Me₂Se ligands form the core 2D sheet, whereas the TFA ligands point out from both sides and are perpendicular to the length of this 2D sheet, as shown in Figure S2b in the Supporting Information. While the pseudo-tetrahedral geometry around Ag1 and Ag2 has an O₃Se environment due to coordination with one terminal TFA, two bridging TFA (μ-η²,η¹- and μ₃-η¹,η¹,η¹-), and one bridging Me₂Se, the other silver atoms are coordinated with either one η²-TFA and two μ-Me₂Se (Ag3) or two η¹-TFA and two μ-Me₂Se (Ag4 and Ag5) to have an O₂Se₂ environment. Besides bridging trifluoroacetate and selenoether ligands, the silver atoms are also connected through short Ag···Ag interactions of 3.14–3.19 Å, a range which is consistent with the reported values on argentophilic interactions.^[28] The Ag–O bond lengths, 2.22–2.78 Å for bridging and 2.24 Å for the terminal trifluoroacetate ligand, compare well with **1**. The Ag–μ-Se bond distances (2.51–2.70 Å) are slightly longer than those found in **1** and **2** where the selenoether ligand is terminal and has a tBu group. The O-Ag-O, Se-Ag-Se and Se-Ag1-O angles in **3** are in the range 75.4–161.7 $^{\circ}$, indicating a distorted tetrahedral environment around the silver center.

The XRD pattern of the as-prepared black powder obtained from the reaction of AgTFA (or AgOTf) and tBu₂Se at room temperature (Figure 2 and Figure S3 in the Supporting Information) exhibits well-crystallized β-Ag₂Se NPs (JCPDS: 01-078-7512). No other phase was observed. An average nanocrystallite size of 35 nm was calculated from the Debye–Scherrer formula. The direct synthesis of β-Ag₂Se NPs at room temperature is important because this phase is stable only at low temperature. The other observation is that only tBu₂Se gives metal selenide materials directly. Other selenoethers such as Et₂Se and Me₂Se usually result in isolable molecular complexes which are stable at room (and even higher) temperature.^[29] tBu₂Se^[17] has previously been used as a source of selenium for the deposition of metal selenide thin films by chemical vapor deposition, though few reports on the use of Et₂Se^[16] and Me₂Se^[15]

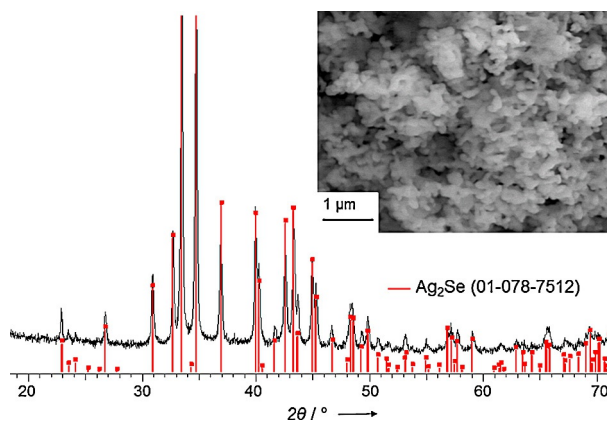


Figure 2. XRD pattern of Ag₂Se NPs obtained from the reaction of AgTFA and tBu₂Se at room temperature. Inset: SEM image of Ag₂Se NPs.

are also available. This difference in behavior among selenoethers can be attributed to a decomposition path via β-hydrogen elimination as well as a weaker C–Se bond in tBu₂Se. Indeed, the C–Se bond becomes weaker with heavier alkyl ligands in the series: Me₂Se > Et₂Se > iPr₂Se > tBu₂Se.^[30] Among silver reagents, the trifluoroacetate (TFA) and triflate (OTf) ligand appear to be much more labile than the iodide ligand. Although the reaction of Me₂Se with a silver salt did not give Ag₂Se NPs at room temperature, its complex [Ag₅(TFA)₅(Me₂Se)₄] (**3**), which was isolated in excellent yield and is stable at room temperature, can be used as a precursor for the synthesis of silver selenide nanomaterials. The TG curve of **3**, recorded under N₂ atmosphere, shows a single-step decomposition in the temperature range 120–315 °C with a residual mass (47.2%) that is consistent with the formation of Ag₂Se (47.8%) as the end product (Figure 3 inset). According to the TGA data, **3** was decomposed in 1-octadecene at 315 °C for 1 h under argon atmosphere. The XRD pattern of the as-prepared black powder, obtained after the usual work-up, exhibited well-crystallized β-Ag₂Se NPs (JCPDS file no. 00-024-1041, Figure 3), although a small amount of silver NPs as con-

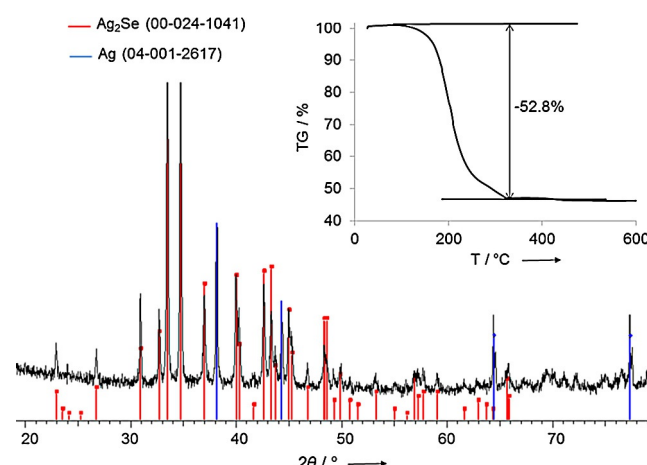


Figure 3. XRD pattern of Ag₂Se NPs obtained from the decomposition of **3** at 315 °C. Inset: TGA curve of **3** recorded under N₂ atmosphere.

tamination was also present (JCPDS file no. 04-001-2617, ~5% as quantified using the reference intensity ratio (RIR) method). As mentioned in the introduction section, only few single-source precursors for Ag_2Se nanomaterials are known in the literature.^[13]

To prepare $\text{Ag}_2\text{Se}-\text{TiO}_2$ nanocomposites, the reaction of AgTFA and $t\text{Bu}_2\text{Se}$ was carried out at room temperature in the presence of different amounts of commercial TiO_2 (P25). After general workup (see Figure S4 in the Supporting Information for a schematic representation), the precipitated powders, varying in color from off-white to black, were isolated by centrifugation, washed twice with ethanol, and dried at room temperature for 24 h. Elemental analysis of these $\text{Ag}_2\text{Se}-\text{TiO}_2$ samples showed 0.36, 0.68, 11.98 and 25.90% Ag, corresponding to 0.13, 0.25, 5 and 15 mol% Ag_2Se , respectively (Table S1 in the Supporting Information). The XRD patterns of these samples show characteristic peaks of Ag_2Se (JCPDS file no. 01-078-7512) and anatase TiO_2 (JCPDS file no. 01-021-1272; Figure S5 in the Supporting Information). These samples also had the rutile TiO_2 (JCPDS file no. 04-003-0648) as a minor phase, which is common in the commercial TiO_2 (P25). As the percentage of TiO_2 increased, the peaks for the anatase phase became more prominent. Next, Brunauer–Emmett–Teller (BET) measurements were carried out on commercial TiO_2 (P25) and $\text{Ag}_2\text{Se}-\text{TiO}_2$ nanocomposites to investigate their surface characteristic (Figure 4a). The obtained isotherms can be identified as type IV which have a small hysteresis loop observed under a relative pressure of 0.85 to 1.00. The surface areas, total pore volumes, and average pore diameters are given in Table S2 in the Supporting Information. When the mol% of Ag_2Se was

low, the BET surface area of the composite increased significantly as compared to the pure TiO_2 . However, when the mol% of Ag_2Se increased to 15%, the surface area decreased to $14.8 \text{ m}^2 \text{ g}^{-1}$ due to the aggregation of Ag_2Se on the TiO_2 . The TEM images show that the composite is composed of well-crystalline Ag_2Se and TiO_2 NPs (Figure 4 inset and Figure S6 in the Supporting Information). X-ray photoelectron spectroscopy (Figure 4 and Figure S7 in the Supporting Information) was used to analyze the valence states of the elements present on $\text{Ag}_2\text{Se}-\text{TiO}_2$ nanocomposites. The binding energies of Ag 3d_{5/2} and Se 3d were found to be 368.1 and 53.5 eV, respectively (Figure 4b and 4c), indicating the presence of these two elements as Ag^{+} and Se^{2-} .^[31] The Ti 2p_{3/2} and Ti 2p_{1/2} peaks at 458.5 eV and 464.4 eV, on the other hand, indicated the presence of Ti^{4+} in the form of TiO_2 (Figure S7 in the Supporting Information). The Tauc plots for the determination of the band gap of the $\text{Ag}_2\text{Se}-\text{TiO}_2$ nanocomposites with different% of Ag_2Se are shown in Figure S8 in the Supporting Information. TiO_2 shows the characteristic spectrum indicating a band gap of about 3.15 eV. However, as the mol% of Ag_2Se increased, the band edge was red-shifted considerably (band gap in the region 3.1–2.9 eV). The increase in absorption is attributed to the narrow band gap of Ag_2Se NPs. With an increased absorption in the visible wavelength, more electron–hole pairs are expected to be generated in the composite under UV/Vis light.

Using the above-mentioned $\text{Ag}_2\text{Se}-\text{TiO}_2$ nanocomposites as photocatalysts, photodegradation experiments of formic acid (FA) were performed under UV and visible light by monitoring with HPLC. All the samples were stirred in the dark for 30 min to reach the adsorption–desorption equilibrium. There was no apparent difference in the adsorption ability of formic acid among the different samples. Pure Ag_2Se showed almost no activity while pure TiO_2 (P25) had a moderate photoactivity under our experimental conditions (Figure 5). The photocatalytic activity of $\text{Ag}_2\text{Se}-\text{TiO}_2$ composites depended strongly on the percentage of Ag_2Se . Generally speaking, the composites with a low content of Ag_2Se (0.01, 0.13 and 0.25%) showed a better UV-induced catalytic activity than TiO_2 . In particular,

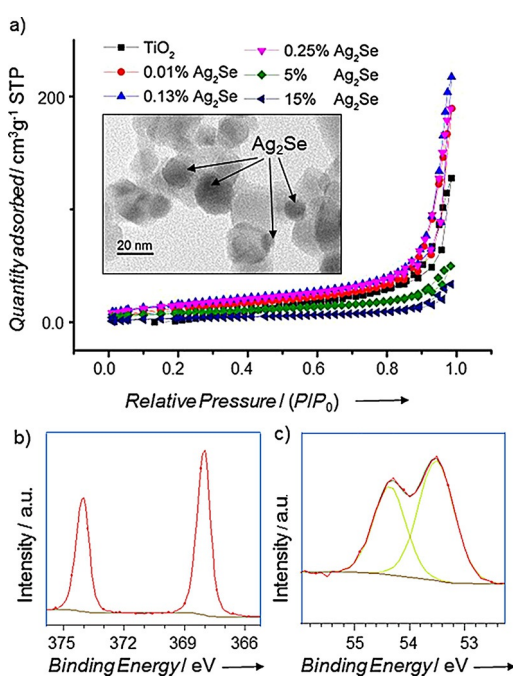


Figure 4. (a) BET isotherms of $\text{Ag}_2\text{Se}-\text{TiO}_2$ nanocomposites with different percentages of Ag_2Se . Inset: Representative TEM image of 0.13% $\text{Ag}_2\text{Se}-\text{TiO}_2$ nanocomposite. XPS spectra showing binding energies of Ag 3d_{5/2} (b) and Se 3d (c) at 368.1 and 53.5 eV, respectively.

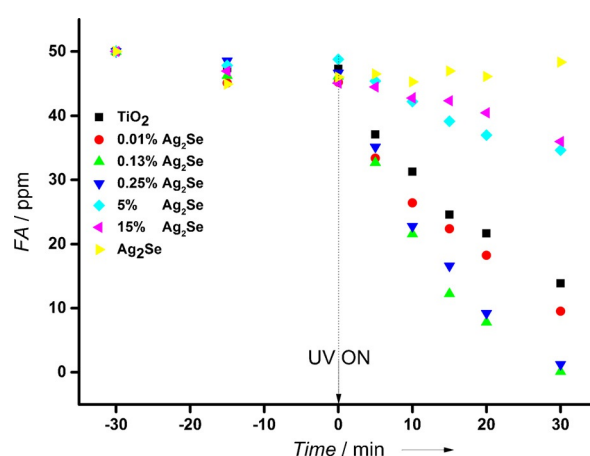


Figure 5. Photodegradation of FA using TiO_2 , Ag_2Se and $\text{Ag}_2\text{Se}-\text{TiO}_2$ with different percentages of Ag_2Se under UV light.

the degradation rate of FA increased as the percentage of Ag₂Se changed from 0.01 mol% to 0.13 mol% but then decreased significantly upon increasing the Ag₂Se content from 0.25 mol% to 15 mol%. The nanocomposite with 0.13% Ag₂Se provided the best catalytic activity and photodegraded formic acid (FA) completely within 30 min under UV-light irradiation. Although these preliminary results do not provide any direct proof of an improved separation of e⁻-h⁺ pairs as proposed previously for the improved efficiency of Ag₂S-TiO₂ composites,^[23] the better activity of the Ag₂Se-TiO₂ nanocomposites (as compared to TiO₂ alone) correlates with their light absorption property and high surface area (Figures S8 and S9 in the Supporting Information).^[22] The Ag₂Se-TiO₂ nanocomposite generates e⁻-h⁺ pairs upon irradiation with UV/Vis light (Eq. S1 and S2 in the Supporting Information). While the electrons react with adsorbed oxygen molecules to form superoxide radicals (O₂^{•-}), the positively charged holes (h⁺) react with HCOOH dissolved in H₂O to generate HCOO[•] radical (Eq. S3 and S4 in the Supporting Information). Formic acid is then converted to CO₂ whereas O₂^{•-} reacts with H⁺ to generate HO₂[•] (Eq. S5 and S6 in the Supporting Information). Previous studies have reported that formic acid degrades catalytically by first forming formate and then CO₂.^[33] As the mol% of Ag₂Se increased, a large amount of Ag₂Se distributed over the surface of TiO₂, leading to inefficient separation of electrons and holes. Besides, because the surface area decreased from 61.3 (0.13 mol% Ag₂Se) to 14.8 m² g⁻¹ (15 mol% Ag₂Se), less active sites were available. With high density of Ag₂Se, the nanocomposites became darker which prevented the TiO₂ to utilize the UV light efficiently. This resulted in the generation of fewer electrons and holes. All the Ag₂Se-TiO₂ composites studied here had no activity under visible light (Figure S10 in the Supporting Information). XPS studies on the 0.13% Ag₂Se-TiO₂ sample were also carried out to know whether there is any change in the surface structure of the catalyst during photodegradation. A comparison of data shown in Figure S7a and S7b in the Supporting Information shows that the amount of Ti³⁺ observed at 457.1 eV is actually increased after the photodegradation experiments. According to Wang et al.^[34] and Fujishima et al.,^[35] Ti⁴⁺ ions on TiO₂ surfaces are converted into Ti³⁺ ions by UV light. The typical XPS peaks of Ag (Figure S7c and S7d in the Supporting Information) did not show any difference before and after the photodegradation, indicating that the as-prepared photocatalyst can be potentially recycled. This was further confirmed by determining the photocatalytic activity of the recycled catalysts which showed good activity even after recycling for 4 times (Figure S11 in the Supporting Information). Detailed studies are currently underway to understand further the synergistic effect between Ag₂Se and TiO₂ components for the aforesaid photocatalytic efficiency and to establish a possible mechanism for it.

In summary, the divergent reactivity of silver reagents with selenoether is presented. While the reaction of AgI and AgTFA with tBu₂Se and Me₂Se, respectively, resulted in the formation of stable molecular complexes, the reaction of AgOTf and AgTFA with tBu₂Se gave Ag₂Se NPs at room temperature. Isolation of [Ag(TFA)(tBu₂Se)]₂ during the course of the latter reac-

tion indicates that the Ag₂Se NPs are formed via this intermediate molecular species. This facile and direct synthetic method of β-Ag₂Se was then extended in the presence of commercial TiO₂ (P25) to prepare Ag₂Se-TiO₂ nanocomposites with different Ag/Ti ratios. The as-prepared Ag₂Se-TiO₂ nanocomposites exhibited excellent photocatalytic activity for the degradation of formic acid under UV light irradiation, the best results being for 0.13% Ag₂Se-TiO₂ nanocomposite, which degraded 50 ppm of formic acid in 30 min.

Experimental Section

Details of the general experimental procedures and a scheme for the synthesis of precursors and Ag₂Se-TiO₂ composites, X-ray crystallography and structure refinement, FT-IR spectra, perspective views on the extended structure of 3, powder XRD, XPS, diffuse reflectance spectra of Ag₂Se and Ag₂Se-TiO₂ composites, experimental setup and graphical plots of photodegradation of formic acid by Ag₂Se-TiO₂ catalysts under UV/Vis light, a correlation diagram between the rate of FA degradation and the specific surface area are given in the Supporting Information. CCDC 1442413 (1), 1442414 (2), and 1442415 (3) contain the supplementary crystallographic data for this paper. These data are provided free of charge by The Cambridge Crystallographic Data Centre.

Acknowledgements

Authors are thankful to Dr. L. Cardenas (XPS), L. Burel (TEM), Y. Aizac (PXRD), P. Mascunan & N. Cristin (elemental analyses) of IRCELYON and O. Boyron and M. Taam (TGA) of C2P2, UCBL.

Keywords: formic acid • molecular precursor • photocatalysis • selenoether • silver selenide • titania

- [1] B. Dong, C. Li, G. Chen, Y. Zhang, Y. Zhang, M. Deng, Q. Wang, *Chem. Mater.* **2013**, *25*, 2503–2509.
- [2] C. Xiao, J. Xu, K. Li, J. Feng, J. Yang, Y. Xie, *J. Am. Chem. Soc.* **2012**, *134*, 4287–4293.
- [3] Y.-P. Gu, R. Cui, Z.-L. Zhang, Z.-X. Xie, D.-W. Pang, *J. Am. Chem. Soc.* **2012**, *134*, 79–82.
- [4] M. Kobayashi, *Solid State Ionics* **1990**, *39*, 121–149.
- [5] D. T. Schoen, C. Xie, Y. Cui, *J. Am. Chem. Soc.* **2007**, *129*, 4116–4117.
- [6] Y. Cui, G. Chen, J. Ren, M. Shao, Y. Xie, Y. Qian, *J. Solid State Chem.* **2003**, *172*, 17–21.
- [7] H. Liu, B. Zhang, H. Shi, Y. Tang, K. Jiao, X. Fu, *J. Mater. Chem.* **2008**, *18*, 2573–2580.
- [8] D. Li, Z. Zheng, Z. Shui, M. Long, J. Yu, K. W. Wong, L. Yang, L. Zhang, W. M. Lau, *J. Phys. Chem. C* **2008**, *112*, 2845–2850.
- [9] C.-N. Zhu, P. Jiang, Z.-L. Zhang, D.-L. Zhu, Z.-Q. Tian, D.-W. Pang, *ACS Appl. Mater. Interfaces* **2013**, *5*, 1186–1189.
- [10] Q. Yao, I. U. Arachchige, S. L. Brock, *J. Am. Chem. Soc.* **2009**, *131*, 2800–2801.
- [11] a) S. Mishra, S. Daniele, *Chem. Rev.* **2015**, *115*, 8379–8448; b) S. Mishra, S. Daniele, L.-G. Hubert-Pfalzgraf, *Chem. Soc. Rev.* **2007**, *36*, 1770–1787.
- [12] a) S. Mishra, E. Jeanneau, M. Rolland, S. Daniele, *RSC Adv.* **2016**, *6*, 1738–1743; b) S. Mishra, E. Jeanneau, S. Mangematin, H. Chermette, M. Poor Kalhor, G. Bonnefont, G. Fantozzi, S. Le Floch, S. Pailhes, S. Daniele, *Dalton Trans.* **2015**, *44*, 6848–6862; c) S. Mishra, V. Mendez, E. Jeanneau, V. Caps, S. Daniele, *Eur. J. Inorg. Chem.* **2013**, 500–510; d) S. Mishra, E. Jeanneau, M.-H. Berger, J.-F. Hochepied, S. Daniele, *Inorg. Chem.* **2010**, *49*, 11184–11189; e) S. Mishra, E. Jeanneau, S. Daniele, V. Mendez, *Dalton Trans.* **2010**, *39*, 7440–7443; f) S. Mishra, S. Daniele, S. Petit, E. Jeanneau, M. Rolland, *Dalton Trans.* **2009**, 2569–2577.

- [13] a) G. K. Kole, K. V. Vivekananda, M. Kumar, R. Ganguly, S. Dey, V. K. Jain, *CrystEngComm* **2015**, *17*, 4367–4376; b) R. K. Sharma, A. Wadawale, G. Kedarnath, D. Manna, T. K. Ghanty, B. Vishwanadh, V. K. Jain, *Dalton Trans.* **2014**, *43*, 6525–6535; c) H. Joshi, K. N. Sharma, V. V. Singh, P. Singh, A. K. Singh, *Dalton Trans.* **2013**, *42*, 2366–2370; d) M. T. Ng, C. Boothroyd, J. J. Vittal, *Chem. Commun.* **2005**, 3820–3822.
- [14] a) K. George, C. H. de Groot, C. Gurnani, A. L. Hector, R. Huang, M. Jura, W. Levason, G. Reid, *Chem. Mater.* **2013**, *25*, 1829–1836; b) S. L. Benjamin, C. H. de Groot, C. Gurnani, A. L. Hector, R. Huang, K. Ignatyev, W. Levason, S. J. Pearce, F. Thomas, G. Reid, *Chem. Mater.* **2013**, *25*, 4719–4724; c) C. H. de Groot, C. Gurnani, A. L. Hector, R. Huang, M. Jura, W. Levason, G. Reid, *Chem. Mater.* **2012**, *24*, 4442–4449; d) A. L. Hector, M. Jura, W. Levason, S. D. Reid, G. Reid, *New J. Chem.* **2009**, *33*, 641–645; e) S. D. Reid, A. L. Hector, W. Levason, G. Reid, B. J. Waller, M. Webster, *Dalton Trans.* **2007**, 4769–4777.
- [15] J. R. Sparks, R. He, N. Healy, M. Krishnamurthi, A. C. Peacock, P. J. Sazio, V. Gopalan, J. V. Badding, *Adv. Mater.* **2011**, *23*, 1647–1651.
- [16] a) N. D. Boscher, C. J. Carmalt, R. G. Palgrave, I. P. Parkin, *Thin Solid Films* **2008**, *516*, 4750–4757; b) N. D. Boscher, C. J. Carmalt, G. Hyett, A. G. Prieto, Q. A. Pankhurst, I. P. Parkin, *J. Mater. Chem.* **2008**, *18*, 1667–1673; c) N. D. Boscher, C. J. Carmalt, A. G. Prieto, Q. A. Pankhurst, R. G. Palgrave, I. P. Parkin, *Eur. J. Inorg. Chem.* **2007**, 4579–4582; d) N. D. Boscher, C. J. Carmalt, I. P. Parkin, *J. Mater. Chem.* **2006**, *16*, 122–127.
- [17] a) N. D. Boscher, C. J. Carmalt, R. G. Palgrave, J. J. Gil-Tomas, I. P. Parkin, *Chem. Vap. Deposition* **2006**, *12*, 692–698; b) N. D. Boscher, C. J. Carmalt, I. P. Parkin, *Eur. J. Inorg. Chem.* **2006**, 1255–1259; c) N. D. Boscher, C. J. Carmalt, I. P. Parkin, *Chem. Vap. Deposition* **2006**, *12*, 54–58; d) T. L. Ng, N. Maung, G. Fan, I. B. Poole, J. O. Williams, A. C. Wright, D. F. Foster, D. J. Cole-Hamilton, *Chem. Vap. Deposition* **1996**, *2*, 185–189.
- [18] R. Daghrir, P. Drougi, D. Robert, *J. Photochem. Photobiol. A* **2012**, *238*, 41–52.
- [19] a) L. L. Zhu, M. H. Hong, G. W. Ho, *Nano Energy* **2015**, *11*, 28–37; b) Y. Zhou, Y. Liu, P. Liu, W. Zhang, M. Xing, J. Zhang, *Appl. Catal. B* **2015**, *170–171*, 66–73; c) X. Li, P. Liu, Y. Mao, M. Xing, J. Zhang, *Appl. Catal. B* **2015**, *164*, 352–359; d) Q. Gu, J. L. Long, H. Q. Zhuang, C. Q. Zhang, Y. G. Zhou, X. X. Wang, *Phys. Chem. Chem. Phys.* **2014**, *16*, 12521–12534; e) B. Tian, R. Dong, J. Zhang, S. Bao, F. Yang, J. Zhang, *Appl. Catal. B* **2014**, *158*, 76–84; f) M. Nasir, Z. Xi, M. Xing, J. Zhang, F. Chen, B. Tian, S. Bagwasi, *J. Phys. Chem. C* **2013**, *117*, 9520–9528; g) S. Bagwasi, B. Tian, J. Zhang, M. Nasir, *Chem. Eng. J.* **2013**, *217*, 108–118; h) C. W. Lai, S. Sreekanthan, *Int. J. Hydrogen Energy* **2013**, *38*, 2156–2166; i) S. Choudhury, R. Sasikala, V. Saxena, D. K. Aswal, D. Bhattacharya, *Dalton Trans.* **2012**, *41*, 12090–12095; j) J. Zhang, Y. Wu, M. Xing, K. L. Sajjad, S. Sajjad, *Energy Environ. Sci.* **2010**, *3*, 715–726; k) D. H. Kim, D. K. Choi, S.-J. Kim, K. S. Lee, *Catal. Commun.* **2008**, *9*, 654–657.
- [20] a) Y. Liu, P. Zhang, B. Tian, J. Zhang, *Catal. Commun.* **2015**, *70*, 30–33; b) J. Yang, H. Bai, Q. Jiang, J. Lian, *Thin Solid Films* **2008**, *516*, 1736–1742.
- [21] J.-C. Lee, T. G. Kim, H.-J. Choi, Y.-M. Sung, *Cryst. Growth Des.* **2007**, *7*, 2588–2593.
- [22] a) D. W. Wang, Y. Li, G. L. Puma, C. Wang, P. F. Wang, W. L. Zhang, Q. Wang, *Appl. Catal. B* **2015**, *168–169*, 25–32; b) C. G. Liu, Z. F. Lei, Y. N. Yang, Z. Y. Zhang, *Water Res.* **2013**, *47*, 4986–4992.
- [23] W. L. Ong, Y.-F. Lim, J. L. T. Ong, G. W. Ho, *J. Mater. Chem. A* **2015**, *3*, 6509–6516.
- [24] Z.-D. Meng, L. Zhu, T. Ghosh, C.-Y. Park, K. Ullah, V. Nikam, W.-C. Oh, *Bull. Korean Chem. Soc.* **2012**, *33*, 3761–3766.
- [25] a) F. R. Knight, R. A. M. Randall, L. Wakefield, A. M. Z. Slawin, J. D. Woolfins, *Dalton Trans.* **2013**, *42*, 143–154; b) M. J. Poropudas, L. Vigo, R. Oilunkaniemi, R. S. Laitinen, *Dalton Trans.* **2013**, *42*, 16868–16877; c) T. Shimizu, M. Kawaguchi, T. Tsuchiya, K. Hirabayashi, N. Kamigata, *J. Org. Chem.* **2005**, *70*, 5036–5044; d) T. Shimizu, M. Kawaguchi, T. Tsuchiya, K. Hirabayashi, N. Kamigata, *Org. Lett.* **2003**, *5*, 1443–1445; e) W. Levason, S. D. Orchard, G. Reid, *Inorg. Chem.* **2000**, *39*, 3853–3859.
- [26] a) H. Ayadi, W. Fang, S. Mishra, E. Jeanneau, G. Ledoux, J. Zhang, S. Daniele, *RSC Adv.* **2015**, *5*, 100535–100545; b) Y. Chen, S. Mishra, G. Ledoux, E. Jeanneau, M. Daniel, J. Zhang, S. Daniele, *Chem. Asian J.* **2014**, *9*, 2415–2421; c) S. Mishra, E. Jeanneau, A.-L. Bulin, G. Ledoux, B. Jouquet, D. Amans, A. Belsky, S. Daniele, C. Dujardin, *Dalton Trans.* **2013**, *42*, 12633–12643; d) S. Mishra, G. Ledoux, E. Jeanneau, S. Daniele, M.-F. Joubert, *Dalton Trans.* **2012**, *41*, 1490–1502; e) S. Mishra, S. Daniele, G. Ledoux, E. Jeanneau, M. F. Joubert, *Chem. Commun.* **2010**, *46*, 3756–3758; f) S. Mishra, J. Zhang, L.-G. Hubert-Pfalzgraf, D. Luneau, E. Jeanneau, *Eur. J. Inorg. Chem.* **2007**, 602–608.
- [27] J. R. Black, N. R. Champness, W. Levason, G. Reid, *Inorg. Chem.* **1996**, *35*, 1820–1824.
- [28] a) S. Mishra, E. Jeanneau, G. Ledoux, S. Daniele, *Inorg. Chem.* **2014**, *53*, 11721–11731; b) S. Mishra, E. Jeanneau, G. Ledoux, S. Daniele, *Dalton Trans.* **2009**, 4954–4961; c) S. Mishra, E. Jeanneau, S. Daniele, G. Ledoux, *Dalton Trans.* **2008**, 6296–6304.
- [29] a) S. Mishra, E. Jeanneau, S. Daniele, *Polyhedron* **2010**, *29*, 500–506; b) C. Gurnani, W. Levason, R. Ratnani, G. Reid, M. Webster, *Dalton Trans.* **2008**, 6274–6282; c) C. Gurnani, M. Jura, W. Levason, R. Ratnani, G. Reid, M. Webster, *Dalton Trans.* **2009**, 1611–1619.
- [30] A. C. Jones, M. L. Hitchman, *Chemical Vapour Deposition: Precursors, Processes and Applications*, Royal Society of Chemistry, **2009**.
- [31] J. P. Ge, S. Xu, L. P. Liu, Y. D. Li, *Chem. Eur. J.* **2006**, *12*, 3672–3677.
- [32] A. Turki, H. Kochkar, C. Guillard, G. Berhault, A. Ghorbel, *Appl. Catal. B* **2013**, *138–139*, 401–415.
- [33] M. F. J. Dijkstra, H. J. Panneman, J. G. M. Winkelmann, J. J. Kelly, A. A. C. M. Beenackers, *Chem. Eng. Sci.* **2002**, *57*, 4895–4907.
- [34] R. Wang, K. Hashimoto, A. Fujishima, M. Chikuni, E. Kojima, A. Kitamura, M. Shimohigoshi, T. Watanabe, *Adv. Mater.* **1998**, *10*, 135–138.
- [35] H. Y. Lee, Y. H. Park, K. H. Ko, *Langmuir* **2000**, *16*, 7289–7293.

Manuscript received: February 5, 2016

Revised: March 24, 2016

Accepted Article published: April 28, 2016

Final Article published: May 19, 2016